Monthly Notices of the ROYAL ASTRONOMICAL SOCIETY LETTERS

Mon. Not. R. Astron. Soc. **417,** L46–L50 (2011) doi:10.1111/j.1745-3933.2011.01117.x

Resolving the nuclear dust distribution of the Seyfert 2 galaxy NGC 3081

C. Ramos Almeida,[1★] M. Sánchez-Portal,[2] A. M. Pérez García,[3,4] J. A. Acosta-Pulido,[3,4] M. Castillo,[2] A. Asensio Ramos,[3,4] J. I. González-Serrano,[5] A. Alonso-Herrero,[6] J. M. Rodríguez Espinosa,[3,4] E. Hatziminaoglou,[7] D. Coia,[2] I. Valtchanov,[2] M. Pović,[8] P. Esquej,[6] C. Packham[9] and B. Altieri[2]

[1]*Department of Physics and Astronomy, University of Sheffield, Sheffield S3 7RH*
[2]*Herschel Science Centre, INSA/ESAC, E-28691 Villanueva de la Cañada, Madrid, Spain*
[3]*Instituto de Astrofísica de Canarias, C/Vía Láctea, s/n, E-38205 La Laguna, Tenerife, Spain*
[4]*Departamento de Astrofísica, Universidad de La Laguna, E-38205 La Laguna, Tenerife, Spain*
[5]*Instituto de Física de Cantabria, CSIC-Universidad de Cantabria, E-39005 Santander, Spain*
[6]*Centro de Astrobiología, INTA-CSIC, E-28850 Madrid, Spain*
[7]*European Southern Observatory, Karl-Schwarzschild-Str. 2, 85748 Garching bei München, Germany*
[8]*Instituto de Astrofísica de Andalucía (CSIC), Apdo. 3004, 18080 Granada, Spain*
[9]*Astronomy Department, University of Florida, 211 Bryant Science Center, PO Box 112055, Gainesville, FL 32611-2055, USA*

Accepted 2011 July 12. Received 2011 July 12; in original form 2011 June 8

ABSTRACT

We report far-infrared (FIR) imaging of the Seyfert 2 galaxy NGC 3081 in the range 70–500 μm, obtained with an unprecedented angular resolution, using the *Herschel Space Observatory* instruments PACS and SPIRE. The 11 kpc (∼70 arcsec) diameter star-forming ring of the galaxy appears resolved up to 250 μm. We extracted IR (1.6–500 μm) nuclear fluxes, that is active nucleus-dominated fluxes, and fitted them with clumpy torus models, which successfully reproduce the FIR emission with small torus sizes. Adding the FIR data to the near- and mid-IR spectral energy distribution (SED) results in a torus radial extent of $R_{\rm o} = 4^{+2}_{-1}$ pc, as well as in a flat radial distribution of the clouds (i.e. the q parameter). At wavelengths beyond 200 μm, cold dust emission at $T = 28 \pm 1$ K from the circumnuclear star-forming ring of 2.3 kpc (∼15 arcsec) in diameter starts making a contribution to the nuclear emission. The dust in the outer parts of the galaxy is heated by the interstellar radiation field (19 ± 3 K).

Key words: galaxies: active – galaxies: nuclei – galaxies: Seyfert – infrared: galaxies – galaxies: individual: NGC 3081.

1 INTRODUCTION

The infrared (IR) spectral energy distribution (SED) of active galactic nuclei (AGN) serves as a sensitive probe of both the dust and the sources that are heating it. Dust grains absorb optical and ultraviolet photons from the AGN and from stars and re-radiate them in the IR range. The *IRAS* and *ISO* satellites revealed that Seyfert galaxies are strong far-IR (FIR) and mid-IR (MIR) emitters (Rodríguez Espinosa, Rudy & Jones 1987; Spinoglio et al. 1995) and that this emission is thermal, and a combination of a warm, a cold and a very cold dust components (Radovich et al. 1999; Pérez García & Rodríguez Espinosa 2001). The warm component is produced by dust heated by either the AGN or circumnuclear starbursts (dust at 120–170 K), the cold dust is heated by stars in the galaxy disc (30–70 K) and the very cold dust is heated by the general interstellar radiation field (15–25 K). With the advent of the *Herschel Space Observatory*[1] (Pilbratt et al. 2010), it is now possible to map the FIR emission of nearby Seyferts galaxies at higher angular resolutions than those previously achieved with the *Spitzer Space Telescope* between 70 and 160 μm. This, together with the unprecedented sensitivities that *Herschel* offers up to 500 μm, allows us to probe their dust distributions at different temperatures. In this Letter, we present new *Herschel* imaging data of the galaxy NGC 3081, which is part of a guaranteed Programme of FIR imaging observations of Seyfert galaxies. The main goal is to characterize their IR SEDs by determining the fractional contributions of the warm, cold and very cold dust components.

★E-mail: C.Ramos@sheffield.ac.uk

[1] *Herschel* is an ESA space observatory with science instruments provided by European-led Principal Investigator consortia and with important participation from NASA.

The galaxy NGC 3081 harbours a Seyfert 2 nucleus, although Moran et al. (2000) reported a spectacular type 1 optical spectrum in polarized light. The galaxy is at a distance of 32.5 Mpc (Buta & Purcell 1998), which corresponds to a spatial scale of 158 pc arcsec^{-1}. This early-type barred spiral is forming stars in a series of nested ring-like features: a nuclear 2.3 kpc diameter ring (hereafter r1), an inner ring of 11 kpc (r2), an outer ring of 26.9 kpc and a pseudo-ring of 33.1 kpc diameter (Buta & Purcell 1998; Buta, Byrd & Freeman 2004; Byrd, Freeman & Buta 2006).

2 OBSERVATIONS

FIR maps of NGC 3081 were obtained with the PACS and SPIRE instruments of the *Herschel Space Observatory*. The data are part of the guaranteed time proposal '*Herschel* imaging photometry of nearby Seyfert galaxies: testing the coexistence of AGN and starburst activity and the nature of the dusty torus' (PI: M. Sánchez-Portal).

The PACS observations were carried out using the 'mini-map' mode, consisting of two concatenated 3-arcmin scan line maps, at 70° and 110° (in array coordinates). This results in a map with a highly homogeneous exposure within the central 1-arcmin area. The PACS beams at 70, 100 and 160 μm are 5.6-, 6.8- and 11.3-arcsec full width half-maximum (FWHM), respectively. With the SPIRE photometer, the three available bands were observed simultaneously using the 'small map' mode, whose area for scientific use is around 5 × 5 arcmin^2. The FWHM beam sizes at 250, 350 and 500 μm are 18.1, 25.2 and 36.9 arcsec, respectively.

We carried out the data reduction with the Herschel Interactive Processing Environment (HIPE) v6.0.1951. For the PACS instrument, we deemed the extended source version of the standard PhotProject reduction script as adequate, given the small angular size of the galaxy. We used the FM v5 photometer response calibration files (Müller et al. 2011). For SPIRE, we applied the standard small map script with the 'naive' scan mapper task, using the calibration data base v6.1. Colour corrections (for PACS, see Poglitsch et al. 2010; please refer to SPIRE Observers' Manual 2011 for the SPIRE ones) are small for blackbodies at the expected temperatures (e.g. Pérez García & Rodríguez Espinosa 2001) and have been neglected. More details on the observations and data processing are given in Sánchez-Portal et al. (in preparation).

The FIR maps of NGC 3081 are shown in Fig. 1. The star-forming ring r2 is clearly resolved in the three PACS images, as well as in the 250-μm SPIRE map. There is a brighter region in the western side of the ring detected at 70, 100, 160 and 250 μm that does not have optical/near-IR (NIR) counterpart in the *HST* images (Buta & Purcell 1998; Buta et al. 2004; Byrd et al. 2006).

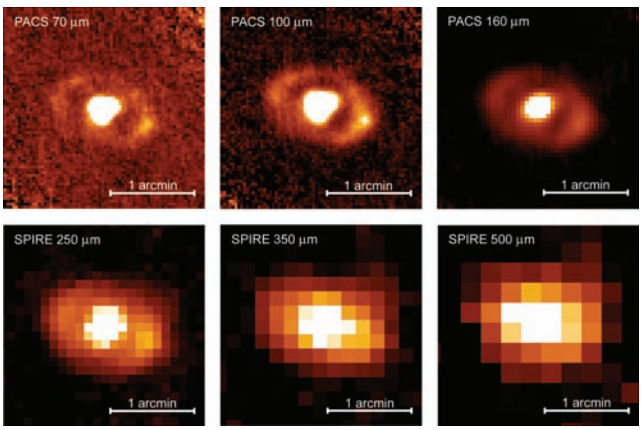

Figure 1. *Herschel* PACS 70-, 100-, and 160-μm images (top) and SPIRE 250-, 350- and 500-μm maps (bottom). North is up and east is to the left. The r2 ring is resolved up to 250 μm.

Table 1. IR nuclear fluxes employed in the fit of NGC 3081 with clumpy torus models. Errors have been obtained by adding quadratically the photometric and PSF subtraction uncertainties.

Instrument	λ_c (μm)	PSF FWHM (arcsec)	PSF FWHM (kpc)	Flux (mJy)	Uncertainty (per cent)
NICMOS	1.6	0.20	0.032	0.22	6
T-ReCS	8.74	0.30	0.047	83	15
VISIR	13.0	0.35	0.055	138	10
T-ReCS	18.3	0.56	0.083	231	25
PACS	70	5.6	0.83	758	30
PACS	100	6.8	1.01	575	30
PACS	160	11.3	1.7	60	30
SPIRE	250	18.1	2.7	488	50
SPIRE	350	25.2	3.7	86	50
SPIRE	500	36.9	5.4	19	60

To study the IR nuclear emission of NGC 3081, we obtained and compiled unresolved fluxes, i.e. either the emission of a point spread function (PSF) component fitted to the data or the emission contained in an aperture diameter equal to the FWHM of the PSF in each band. In the case of the FIR, we used GALFIT 2D fitting (Peng et al. 2002) to obtain the unresolved fluxes. For the PACS images, we fitted a PSF component, which we identified with the nuclear flux, a Sérsic profile of $R_e \sim$ 7–18 arcsec and a fainter and larger Sérsic component of $R_e \sim$ 45–60 arcsec, where R_e is the half-light radius given by GALFIT. For the SPIRE data we only fitted a PSF component and a Sérsic profile of $R_e \sim$ 75–90 arcsec. We also tried this simpler PSF + Sérsic fit with the PACS images, but the three-component model results in smaller residuals and values of the reduced χ^2 (0.002 for PACS and 0.02 for SPIRE). All the fitted Sérsic components have indices between 0.4 and 0.8 (i.e. disc-like) and do not reproduce the r2 ring, which is a residual of the fits. The PSF input functions are the empirical ones from PACS and SPIRE (Lutz 2010; Sibthorpe et al. 2011).

In addition, we compiled the highest angular resolution NIR and MIR data from the literature to construct the nuclear SED. Sub-arcsecond resolution MIR images of NGC 3081 (0.30 arcsec at 8.74 μm and 0.56 arcsec at 18.3 μm) were obtained using the camera/spectrograph T-ReCS on the Gemini South Telescope. The unresolved T-ReCS fluxes from Ramos Almeida et al. (2009) are reported in Table 1, together with an additional nuclear flux at 13.04 μm from VISIR on the VLT with similar resolution as the T-ReCS data (Gandhi et al. 2009). In the NIR, we use the nuclear flux obtained from the NICMOS 1.6-μm image reported in Quillen et al. (2001).

In Table 1, we report the unresolved NIR, MIR and FIR fluxes, their uncertainties and the angular resolution at each wavelength. The FIR errors are the result of adding quadratically the photometric accuracies [5 per cent for PACS at 70 and 100 μm and 10 per cent at 160 μm (Müller et al. 2010) and 7 per cent for SPIRE (SPIRE Observers' Manual 2011)] and the PSF flux determination uncertainties. The latter are the dominant source of error and account for the variations in the PSF fluxes associated to the GALFIT fitting in each band.

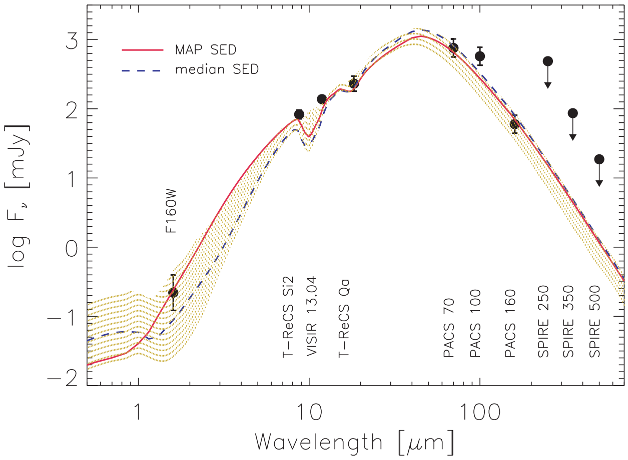

Figure 2. Rest-frame IR SED of NGC 3081 (dots). Solid and dashed lines are the 'best fit' to the data (MAP) and the model described by the median of the posteriors, respectively. The shaded region indicates the range of models compatible with the observations at the 2σ level. The SPIRE fluxes are set as upper limits in the fit.

3 NUCLEAR SED MODELLING

In a recent series of papers (Ramos Almeida et al. 2009, 2011; Alonso-Herrero et al. 2011), we fitted the nuclear NIR and MIR emission of Seyfert galaxies with the clumpy torus models of Nenkova et al. (2008) and were able to nicely constrain the torus parameters, including the torus radial extent, $Y = R_o/R_d$, where R_o and R_d are the outer and inner radius[2] of the toroidal distribution of clumps, respectively. However, it is not clear if the lack of FIR high angular resolution data, which probe cooler dust, might bias the fits to smaller torus sizes. In the context of the Nenkova models, clouds are heated by the AGN radiation (directly illuminated) and by other clouds (indirectly illuminated), and each clump contains a range of temperatures itself. The temperature of the dust within the torus scales with the square root of the distance to the sublimation radius. Thus, a distribution of clumps with $Y \sim 100$ will include directly illuminated clumps at temperatures ranging from T_d to ∼150 K, as well as shadowed clumps with temperatures of a few Kelvin only. To test how the addition of FIR data affects the fits described above, here we use *Herschel* PACS and SPIRE nuclear fluxes combined with NIR and MIR data of the galaxy NGC 3081 and fitted them with clumpy torus models. In general, the latter models appear to reproduce better the IR emission of nearby AGN than smooth torus models (e.g. Alonso-Herrero et al. 2003; Mullaney et al. 2011) although there is not a general consensus on the dust distribution yet. Indeed, in forthcoming publications based on guaranteed time *Herschel* observations of AGN we plan to use the smooth torus models described in Fritz, Franceschini & Hatziminaoglou (2006) and Hatziminaoglou et al. (2008) to compare with the results obtained with clumpy torus models.

We constructed the nuclear 1.6–500 μm SED of NGC 3081 (see Fig. 2) using the nuclear fluxes reported in Table 1. The unresolved NIR and MIR components correspond to a physical region of <85 pc in diameter and thus are likely be dominated by emission from the AGN dusty torus. The nuclear FIR fluxes of NGC 3081, on the other hand, come from regions with sizes of ∼1 kpc in the case of PACS and between 2.7 and 5.4 kpc for SPIRE. These regions are much larger than the physical scales responsible for the NIR and MIR unresolved emission. Indeed, the SPIRE nuclear fluxes include emission from the inner ring of 2.3-kpc diameter (r1), and, consequently, we consider them as upper limits in the fit (see Fig. 2). The PACS fluxes exclude r1, but may include other sources of nuclear emission apart from the torus. This contamination might affect the SED shape and, consequently, the resulting torus parameters. However, here we work under the assumption that the torus is the dominant source of unresolved emission up to 160 μm. Although Deo et al. (2009) showed that, in general, the AGN continuum of Seyfert 2 galaxies drops rapidly beyond 20 μm, NGC 3081 is one of the galaxies in their sample with the smallest starburst-to-AGN ratios at 30 μm. Indeed, the *Spitzer* IRS flux measurement that they reported for this galaxy, 1.09 Jy, nicely matches our fitted torus models (see below).

The clumpy dusty torus models of Nenkova et al. (2008) are characterized by six parameters, which are described in Table 2. Here we use an interpolated version of the Nenkova models to fit the IR nuclear fluxes reported in Table 1 (considering the SPIRE fluxes as upper limits) using our Bayesian inference tool BAYESCLUMPY (Asensio Ramos & Ramos Almeida 2009) and the uniform priors described in Table 2. The result of the SED fitting are the posterior distributions of the model parameters (Fig. 3), but we can translate these results into a single SED. In Fig. 2, we plot the model that better fits the IR data, i.e. the maximum a posteriori (MAP) model, and the model described by the medians of the six posteriors resulting from the fit (see Table 2). The nuclear NIR, MIR and FIR emission of NGC 3081, at least up to 160 μm, is successfully reproduced by a relatively broad clumpy torus ($\sigma = 57°$) with an average number of clouds $N_0 = 5$ along the radial equatorial direction, and with a close to edge-on inclination $i = 71°$.

In Ramos Almeida et al. (2011; hereafter RA11), we fitted the NIR/MIR nuclear SED of NGC 3081 using the same models as here and obtained σ, N_0 and i values which agree with those reported here. On the other hand, the torus radial extent, Y, and the index of the clouds radial distribution, q, change significantly when adding the FIR data. The sensitivity of the SED to q for small values of Y is highly reduced. This is because for small tori the SED shape does not change noticeably when the clumps are either distributed along the whole extent of the torus ($q = 0$) or highly concentrated in its inner part ($q = 2$–3). Here we obtain $q = 0.2$, which is characteristic of a flat cloud distribution, and a torus radial extent $Y = 84$, whereas in RA11 the resulting values for NGC 3081 were $q = 2.3$ and $Y = 22$. However, while in RA11 we imposed $Y = [5, 30]$ as a prior, in this work we use $Y = [5, 100]$ to take into account cold dust within larger scales. We did the test of fitting only the NIR and MIR data using the same priors shown in Table 2 and obtained $Y = 35$, with the other parameters resulting in similar values as those reported in RA11. We also performed the fit by considering both the PACS and SPIRE fluxes as upper limits, and the results are practically the same as those from the NIR/MIR fit. Summarizing, including the FIR data in the fit of NGC 3081 results in a relatively large torus radial extent and flattens the cloud distribution.

Using the median value of A_V^{LOS} (in the following we will refer to median values in order to give uncertainties at the 68 per cent confidence level, which are defined around the median) reported in Table 2, we can derive the column density using the Galactic dust-to-gas ratio ($N_{\mathrm{H}}^{\mathrm{LOS}} = 1.9 \times 10^{21} A_V{}^{\mathrm{LOS}}$; Bohlin, Savage & Drake 1978). This gives $N_{\mathrm{H}}^{\mathrm{LOS}} = 4.1^{+2.2}_{-1.6} \times 10^{23}\ \mathrm{cm}^{-2}$, which is compatible with the value derived from *ASCA* X-ray observations of NGC

[2] The inner radius is defined by the dust sublimation temperature ($T_d \sim$ 1500 K).

Table 2. Clumpy model parameters and $A_V^{\rm LOS}$ derived from them. Columns 1 and 2 give the parameter description and abbreviation used in the text. Column 3 indicates the input ranges considered for the fit (i.e. the uniform priors). Finally, columns 4 and 5 list the medians and modes of the posterior distributions shown in Fig. 3.

Parameter	Abbreviation	Interval	Fitting results Median	Mode
Width of the angular distribution of clouds	σ	[15°, 75°]	$48°^{+12}_{-19}$	57°
Radial extent of the torus ($R_{\rm o}/R_{\rm d}$)	Y	[5, 100]	76^{+14}_{-19}	84
Number of clouds along the radial equatorial direction	N_0	[1, 15]	8^{+4}_{-3}	5
Power-law index of the radial density profile	q	[0, 3]	$0.4^{+0.4}_{-0.3}$	0.2
Inclination angle of the torus	i	[0°, 90°]	$54°^{+19}_{-25}$	71°
Optical depth per single cloud	τ_V	[5, 150]	59^{+18}_{-27}	72
A_V produced by the torus along the line of sight (LOS)	$A_V^{\rm LOS}$	–	214^{+117}_{-85} mag	162 mag

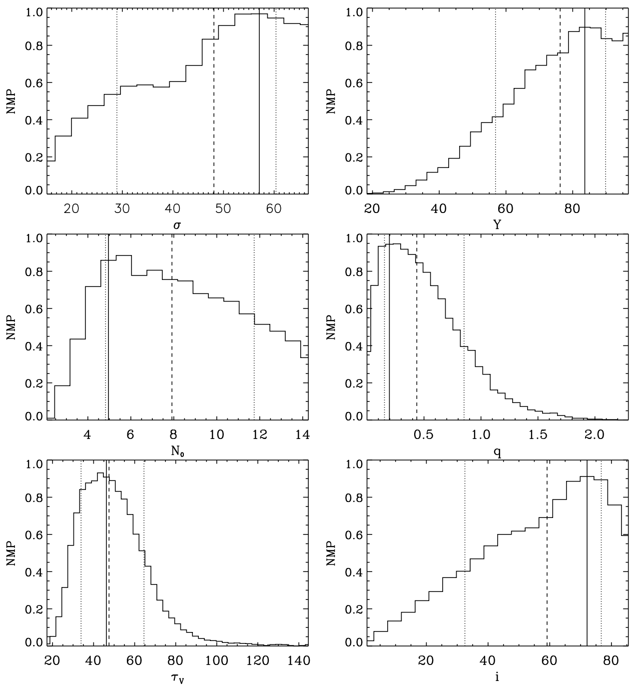

Figure 3. Normalized marginal posteriors (NMPs) resulting from the fit of NGC 3081. Solid and dashed vertical lines represent the modes and medians of each NMP, respectively, and dotted vertical lines indicate the 68 per cent confidence level for each parameter around the median.

3081 ($N_{\rm H}^{\rm X-rays} = 6.3 \pm 0.4 \times 10^{23}$ cm^{-2}; Levenson et al. 2009). The AGN bolometric luminosity can be obtained from the vertical shift applied to the models to fit the data: $L_{\rm bol}^{\rm AGN} = 2.1^{+1.8}_{-0.8} \times 10^{43}$ erg s^{-1} and can be directly compared with the 2–10 keV intrinsic luminosity derived from the *ASCA* data, after applying a bolometric correction factor of 20 (Elvis et al. 1994): $L_{\rm bol}^{\rm X} = 1.0 \pm 0.2 \times 10^{44}$ erg s^{-1}. The difference between $L_{\rm bol}^{\rm AGN}$ and $L_{\rm bol}^{\rm X}$ is smaller than the one found by RA11 for NGC 3081.

As explained before, the outer size of the toroidal distribution of clouds is defined as $R_{\rm o} = YR_{\rm d}$, where $R_{\rm d}$ scales with $L_{\rm bol}^{\rm AGN}$. Thus, $R_{\rm o} = 0.4Y(L_{\rm bol}^{\rm MIR}/10^{45})^{0.5}$ pc $= 4^{+2}_{-1}$ pc, which includes dust at very different temperatures (from $T_{\rm d}$ to a few Kelvin). This value is larger than the torus radius obtained from the fit of NIR and MIR data only ($R_{\rm o} = 0.7 \pm 0.3$ pc; see RA11). Finally, we can calculate the torus covering factor, $C_{\rm T}$. Broader tori with more clumps will have larger covering factors and vice versa. According to our modelling, $C_{\rm T} = 0.8^{+0.5}_{-0.3}$, which is among the typical values found for Seyfert 2 galaxies in RA11, and it is compatible with X-ray studies (e.g. Ricci et al. 2011).

4 CIRCUMNUCLEAR AND EXTENDED DUST PROPERTIES

As explained above, the unresolved component of the SPIRE data includes the inner ring r1 apart from the active nucleus (note the clear bump of emission at $\lambda > 160$ µm in Fig. 2). To characterize the heating source of this component, we have extracted fluxes in an aperture equal to the maximum size of the PSF in the SPIRE bands (i.e. the FWHM at 500 µm; 36.9 arcsec) and then subtracted the galaxy background emission measured in an adjacent annulus (first row in Table 3). The blue dotted line in Fig. 4 corresponds to the best-fitting torus model (MAP), and by subtracting it from the latter

Table 3. PACS and SPIRE flux densities of NGC 3081 in mJy. The total fluxes were obtained in apertures big enough to include the whole galaxy emission in each band.

Aperture	F_{70}	F_{100}	F_{160}	F_{250}	F_{350}	F_{500}
36.9 arcsec	2124	2424	1627	552	187	61
Total flux	2432	3210	3164	1950	757	284

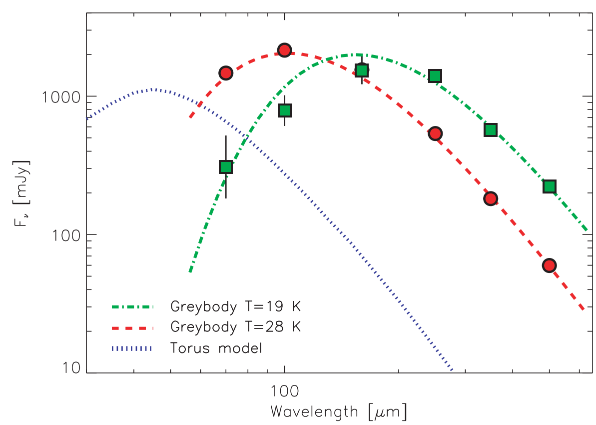

Figure 4. Fit of the circumnuclear emission of NGC 3081 with a greybody of $T = 28 \pm 1$ K (red dashed line). The green dot–dashed line corresponds to the fit of the disc emission with a greybody of $T = 19 \pm 3$ K.

fluxes, we can isolate the dust emission that is not related to the torus (red dots). The best fit that we get for the latter component is a greybody of emissivity $\epsilon = 2$ and temperature $T = 28 \pm 1$ K, which is typical of dust heated by young stars in the galaxy disc. Indeed, based on *HST* images, Buta et al. (2004) detected ∼350 diffuse bright clusters of $R_c \sim 11$ pc, with stellar populations younger than 10 Myr. In a similar way, we can determine the temperature of the dust in the galaxy disc by subtracting the fluxes obtained in the 36.9 arcsec aperture from the total galaxy fluxes reported in Table 3 (green squares). Fig. 4 shows the fit of this component with a greybody of $\epsilon = 2$ and $T = 19 \pm 3$ K, which is compatible with dust heated by the interstellar radiation field.

We integrated the emission of the two previous components and obtained their IR luminosities (1–1000 μm): $L_{\rm IR}^{\rm circ} = 1.4 \times 10^9\,{\rm L}_{\odot}$ and $L_{\rm IR}^{\rm disc} 2.2 \times 10^9\,{\rm L}_{\odot}$. Following the equation $M_{\rm d} = 7.9 \times 10^{-5} (T/40)^{-6} L_{\rm IR}\,{\rm L}_{\odot}$ (${\rm M}_{\odot}$) from Klaas & Elsässer (1993), we can estimate the dust masses as in Radovich et al. (1999). We obtain a mass of $0.9 \times 10^6\,{\rm M}_{\odot}$ for the circumnuclear dust at $T = 28$ K and $1.6 \times 10^7\,{\rm M}_{\odot}$ for the disc. The dust mass content of NGC 3081 is ∼5 times smaller than the value reported by Radovich et al. (1999), for the disc of the star-forming Seyfert 2 NGC 7582. This mass ratio is twice that of the H I masses ($M_{\rm H\,I} \propto d^2 S_\upsilon(21\,{\rm cm})\delta\upsilon$; Giovanelli & Haynes 1988), but it is consistent with the relative content of virial mass in both galaxies.

5 CONCLUSIONS

The FIR nuclear luminosity of NGC 3081 (on scales ⩽1.7 kpc in diameter) can be reproduced by warm/cold dust within a clumpy torus heated by the AGN. On larger scales (5.4 kpc), the IR emission corresponds to a cold dust component at $T = 28 \pm 1$ K heated by young stars in the galaxy disc, likely located in the r1 star-forming ring. On the other hand, the dust located in the outer parts of the galaxy is heated by the interstellar radiation field (19±3 K). These components are coincident with the findings of IR studies of nearby Seyfert galaxies (Radovich et al. 1999; Pérez García & Rodríguez Espinosa 2001; Bendo et al. 2010).

In our previous work using clumpy torus models we fitted the NIR-to-MIR SED of NGC 3081, among other Seyfert galaxies, with an interpolated version of the Nenkova et al. (2008) models. In this Letter, we have repeated the fit after adding the nuclear *Herschel* fluxes to the SED. The FIR data provide information about cooler dust within the torus, resulting in a relatively large value of the torus outer radius and a flat radial distribution of the clumps.

ACKNOWLEDGMENTS

CRA acknowledges financial support from STFC (ST/G001758/1) and from the Spanish Ministry of Science and Innovation (MICINN) through project Consolider-Ingenio 2010 Programme grant CSD2006-00070: First Science with the GTC. AMPG and JIGS acknowledge the Spanish Ministry of Science and Innovation (MICINN) through project AYA2008-06311-C02-01/02. AAR acknowledges the Spanish Ministry of Science and Innovation through projects AYA2010-18029 (Solar Magnetism and Astrophysical Spectropolarimetry). AAH and PE acknowledges support from the Spanish Plan Nacional de Astronomía y Astrofísica under grant AYA2009-05705-E. MP acknowledges Junta de Andalucía and Spanish Ministry of Science and Innovation through projects PO8-TIC-03531 and AYA2010-15169. PACS has been developed by a consortium of institutes led by MPE (Germany) and including UVIE (Austria); KU Leuven, CSL, IMEC (Belgium); CEA, LAM (France); MPIA (Germany); INAF-IFSI/OAA/OAP/OAT, LENS, SISSA (Italy); IAC (Spain). This development has been supported by the funding agencies BMVIT (Austria), ESA-PRODEX (Belgium), CEA/CNES (France), DLR (Germany), ASI/INAF (Italy) and CICYT/MCYT (Spain). SPIRE has been developed by a consortium of institutes led by Cardiff University (UK) and including University of Lethbridge (Canada); NAOC (China); CEA, LAM (France); IFSI, University of Padua (Italy); IAC (Spain); Stockholm Observatory (Sweden); Imperial College London, RAL, UCL-MSSL, UKATC, University of Sussex (UK); and Caltech, JPL, NHSC, University of Colorado (USA). This development has been supported by national funding agencies: CSA (Canada); NAOC (China); CEA, CNES, CNRS (France); ASI (Italy); MCINN (Spain); SNSB (Sweden); STFC (UK) and NASA (USA). We finally acknowledge the anonymous referee for the useful comments.

REFERENCES

Alonso-Herrero A. et al., 2003, AJ, 126, 81
Alonso-Herrero A. et al., 2011, ApJ, 736, 82
Asensio Ramos A., Ramos Almeida C., 2009, ApJ, 696, 2075
Bendo G. J. et al., 2010, A&A, 518, L65
Bohlin R. C., Savage B. D., Drake J. F., 1978, ApJ, 224, 132
Buta R., Purcell G. B., 1998, AJ, 115, 484
Buta R. J., Byrd G. G., Freeman T., 2004, AJ, 127, 1982
Byrd G. G., Freeman T., Buta R. J., 2006, AJ, 131, 1377
Deo R. P. et al., 2009, ApJ, 705, 14
Elvis M. et al., 1994, ApJS, 95, 1
Fritz J., Franceschini A., Hatziminaoglou E., 2006, MNRAS, 366, 767
Gandhi P. et al., 2009, A&A, 502, 457
Giovanelli R., Haynes M. P., 1988, Galactic and Extragalactic Radio Astronomy, 2nd edn. Springer, New York
Hatziminaoglou E. et al., 2008, MNRAS, 386, 1252
Klaas U., Elsässer H., 1993, A&A, 280, 76
Levenson N. A. et al., 2009, ApJ, 703, 390
Lutz D., 2010, 'PACS Photometer PSF', PICC-ME-TN-033, version 1.01
Moran E. C. et al., 2000, ApJ, 540, L73
Mullaney J. R. et al., 2011, MNRAS, 414, 1082
Müller T. et al., 2011, PACS Photometer – Point Source Flux Calibration, PICC-ME-TN-037 v1.0
Müller T. et al., 2011, PACS Photometer – Point/Compact Source Observations: Mini Scan-Maps and Chop-Nod, PICC-ME-TN-036 v1.0
Nenkova M. et al., 2008, ApJ, 685, 147
Peng C. Y. et al., 2002, AJ, 124, 266
Pérez García A. M., Rodríguez Espinosa J. M., 2001, ApJ, 557, 39
Pilbratt G. J. et al., 2010, A&A, 518, L1
Poglitsch A. et al., 2010, A&A, 518, L2
Quillen A. C. et al., 2001, ApJ, 547, 129
Radovich M. et al., 1999, A&A, 348, 705
Ramos Almeida C. et al., 2009, ApJ, 702, 1127
Ramos Almeida C. et al., 2011, ApJ, 731, 92 (RA11)
Ricci C. et al., 2011, A&A, preprint (arXiv:1104.3676v2)
Rodríguez Espinosa J. M., Rudy R. J., Jones B., 1987, ApJ, 312, 555
Sibthorpe B. et al., 2011, 'SPIRE Beam Model Release Note', version 1.1
Spinoglio I. et al., 1995, ApJ, 453, 616
SPIRE Observers' Manual, 2011, v2.3, Herschel Science Centre, HERSCHEL-DOC-0798

This paper has been typeset from a TEX/LATEX file prepared by the author.